Research Article

Two-Dimensional Beampattern Synthesis for Polarized Smart Antenna Array and Its Sparse Array Optimization

Zhikun Chen ⬚, Tao Li, Dongliang Peng, and Kang Du

School of Automation, Hangzhou Dianzi University, Xiasha Higher Education Zone, 2nd Street, Hangzhou 310018, China

Correspondence should be addressed to Zhikun Chen; czk@hdu.edu.cn

Polarized smart antenna array has attracted considerable interest due to its capacity of matched reception or interference suppression for active sensing systems. Existing literature does not take full advantage of the combination of polarization isolation and smart antennas and only focuses on uniform linear array (ULA). In this paper, an innovative synthesis two-dimensional beampattern method with a null that has cross-polarization for polarized planar arrays is proposed in the first stage. This method aims to further enhance the capability of interference suppression whose optimization problem can be solved by second-order conic programming. In the second stage, a new sparse array-optimized method for the polarized antenna array is proposed to reduce the high cost caused by the planar array that is composed of polarized dipole antennas. Numerical examples are provided to demonstrate the advantages of the proposed approach over state-of-the-art methods.

1. Introduction

Smart antennas increase the capacity of communication systems by improving signal-to-noise ratio (SNR) in mobile communications [1, 2]. Adaptive array coherently combines multipath components of the desired signal and null interfering signals from different directions of arrival from the desired signal. In terms of the capability to match reception and suppress interference, the adaptive array is also applied in modern radar systems [3, 4]. However, this kind of conventional space-time adaptive technology has its own limitations, especially in intentional interference. Thus, polarization diversity is a potential solution [5–8]. Polarization diversity not only reflects complete information on electromagnetic waves of targets but also is an additional degree of freedom that can be exploited in response to dynamic environments. Polarization diversity can maximize the received SNR when matching the target polarization and can isolate the interfering signal from the desired signal when cross-polarizing the interfering signal. Considering this advantage, two synthesizing methods are introduced to design an electromagnetic beam with desired power and polarization [5, 9]. According to the literature [5, 9], dipole antennas are suitable for generating arbitrary polarization with a pair of orthogonal far-field electric vectors. Polarized arrays can transmit a beampattern that can be selected freely to design a desired null and polarization around areas of interest. An effective approach to suppress strong interference is based on the principle of polarization mismatch factor; that is, the polarization in the specific region that corresponds to the direction of strong interference is crossed to that of strong interference to isolate the interference signal energy at the receiver as much as possible. Thus, the beamforming for polarized antenna array has become a popular research topic in recent years [10, 11]. However, most existing literature studies on polarized beamforming are only based on a simple uniform linear array (ULA) due to the high-dimensional weight matrix. A Fábry–Perot cavity antenna with a reconfigurable partially reflecting surface is proposed to produce dual-polarized 2D beams [12]. Realizing the compatibility of this kind of antenna with space-time adaptive processing technology based on ULA is difficult, additionally, for the planar array composed of polarized dipole antennas. A planar array generally comprises dozens or even hundreds of dipole antenna elements at the cost of high-precision hardware for its

implementation [13]. Thus, sparse array design is essential for satisfying the function of using a finite number of elements to realize the polarization vector beam.

Unlike the conventional phase arrays, the sparse array design for polarized smart array must be a constrained optimization problem [14–18]. One particular constraint is polarization matching, which is an inequality constraint. This constraint means that the optimization problem cannot be solved by the single-objective optimization algorithm. Transforming constraint optimization into multiobjective optimization or adding a penalty function in the fitness function is necessary to solve such a constrained optimization problem [19]. Scholars proposed multiobjective algorithms based on a new evolutionary pattern in recent decades. According to [20], the optimization problem with inequality constraint can be transformed into a multiobjective optimization problem. This problem can be solved using the multiobjective differential evolution (MODE) algorithm. In this work, the multioptimization design of a sparse antenna array for polarized smart antennas is addressed following the MODE algorithm.

The rest of this paper is organized as follows. The signal model for the polarized antenna is introduced in Section 2. Second-order cone programming (SOCP) is presented in Section 3 to solve the optimization problem of the 2D polarized beampattern design. Multiobjective differential evolution is applied to solve the multiobjective optimization problem in Section 4. Numerical simulations are presented in Section 5, and the conclusions are presented in Section 6.

2. Signal Model

2.1. Representation of Polarization State. The polarization state of the far-field electric field can be characterized by its polarization ellipse. The polarization ellipse is the most frequently used representation of polarization states. The polarization angle can be defined as the angle between the major axis of the ellipse and a reference vector to orient the ellipse in space. In the ellipse, the polarization state can be defined by its polarization axial ratio and angle. The electric field produces an ellipse over one period when plotted on a 2D plane normal to the propagation direction. The polarization axial ratio is the ratio of the major to minor axes of the ellipse. This ratio also determines the circularity (low axial ratio) and linearity (high axial ratio) of the polarization.

In Figure 1, α is called the orientation angle (the angle between the major semiaxis of the ellipse and the H-axis) and β is the ellipse angle (the angle measuring the ratio of the two semiaxes). If the amplitude of the electromagnetic wave is ignored, then the polarization state of electromagnetic waves can be characterized by parameter pair (α, β). This state is called the geometric descriptor of polarization state. When $\beta = 0$, the resultant polarization is linear; moreover, $\alpha = 0$ provides a horizontal polarization and $\beta = (\pi/2)$ leads to a vertical polarization. However, for $\beta = \pm (\pi/4)$, the resultant polarization is circular for any orientation angle α.

The mathematical relationship between electric field and polarization ellipse parameters can be expressed as follows:
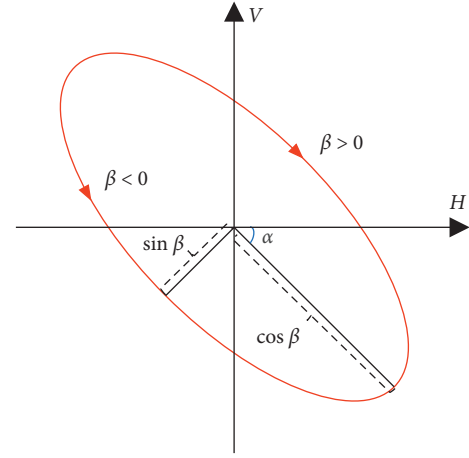

FIGURE 1: Polarization ellipse.

$$
\begin{aligned}
E &= A \cdot \begin{bmatrix} \cos\alpha & -\sin\alpha \\ \sin\alpha & \cos\alpha \end{bmatrix} \cdot \begin{bmatrix} \cos\beta & j\sin\beta \end{bmatrix}^T \\
&= A \cdot \begin{bmatrix} \cos\alpha\cos\beta - j\sin\alpha\sin\beta \\ \sin\alpha\cos\beta + j\cos\alpha\sin\beta \end{bmatrix} \\
&= \begin{bmatrix} E^H \\ E^V \end{bmatrix}.
\end{aligned} \tag{1}
$$

In (1), the first item on the right is the rotation matrix, and second one is the ellipticity vector; $A = \sqrt{|E^H|^2 + |E^V|^2}$ represents the energy of an electromagnetic wave.

The complex electric field vector can also be defined as follows:

$$
\mathbf{E} = A \begin{bmatrix} \cos\gamma \\ \sin\gamma e^{j\delta} \end{bmatrix}. \tag{2}
$$

In (2), $\tan\gamma = (A_H/A_V)$ represents the ratio between the amplitude of vertical and horizontal channel electric fields, $\delta = \phi_V - \phi_H$ is the phase difference between the vertical and the horizontal channel components, $\gamma \in [0, (\pi/2)]$, and $\delta \in [0, 2\pi]$. Given that the energy information of electromagnetic wave is not considered in this study, the parameter pair is reversible to the polarization state of electromagnetic wave. Thus, the parameter pair can be called the phase descriptor of polarization state of electromagnetic wave. If $(E^H/E^V) = \gamma e^{j\delta}$ and $(E^H)^2 + (E^V)^2 \neq 0$, then the relationship between geometric and phase descriptors can be expressed as follows:

$$
\alpha = \tan^{-1}\left(\frac{-2\gamma\cos\delta}{1-\gamma^2}\right),
$$

$$
\beta = \arcsin\frac{\sqrt{1-\left(2\gamma/(1+\gamma)^2\right)\sin\delta} - \sqrt{1+\left(2\gamma/(1+\gamma)^2\right)\sin\delta}}{2}. \tag{3}
$$

2.2. Polarized Vector Array Response. Suppose $\mathbf{r}$ is a unit vector representing a spatial direction in $\mathbb{R}^3$, which can be expressed as follows:

$$\mathbf{r} = \begin{bmatrix} \sin\theta\cos\varphi & \sin\theta\sin\varphi & \cos\theta \end{bmatrix}^T. \tag{4}$$

In (4), $\theta \in [-\pi/2, \pi/2]$ is pitch, and $\varphi \in [0, 2\pi]$ is azimuth:

$$\widehat{\theta} \triangleq \frac{\partial r}{\partial \theta} = \begin{bmatrix} \cos\theta\cos\varphi & \cos\theta\sin\varphi & -\sin\theta \end{bmatrix}^T,$$

$$\widehat{\varphi} \triangleq \frac{1}{\sin\theta}\frac{\partial r}{\partial \varphi} = \begin{bmatrix} -\sin\varphi & \cos\varphi & 0 \end{bmatrix}^T, \tag{5}$$

where $(\mathbf{r}, \widehat{\theta}, \widehat{\varphi})$ can be described as a right-hand coordinate system, as shown in Figure 2.

If the plane wave is traveling along the $\overrightarrow{\mathbf{r}}$-direction, the electric field is orthogonal to τ and lies in the plane spanned by $(\mathbf{r}_H, \mathbf{r}_V)$. Polarized vector antennas comprising orthogonal electric and magnetic dipoles are considered. In this spatial coordinate system $(\mathbf{r}_H, \mathbf{r}_V)$, each of the six dipoles has the following responses (ignoring a common constant that is determined by the antenna parameters and the distance to the antenna).

In this paper, we simplified the representation of polarization state in the coordinate system and only considered the electric field and magnetic field along the x direction. Thus, the polarized antennas have the responses as follows (regardless of the antenna parameters and the distance to the antenna):

$$\mathbf{v}_x^E(\mathbf{r}) = \begin{bmatrix} -\sin\varphi & \cos\theta\cos\varphi \end{bmatrix},$$

$$\mathbf{v}_x^M(\mathbf{r}) = \begin{bmatrix} \cos\theta\cos\varphi & \sin\varphi \end{bmatrix}. \tag{6}$$

If the antenna only comprises electric and magnetic dipole elements along $\mathbf{r}$, then the response is as follows:

$$\mathbf{V}(\mathbf{r}) = \begin{bmatrix} \mathbf{v}_x^E & \mathbf{v}_x^M \end{bmatrix}^T. \tag{7}$$

Moreover, for a given antenna response $\mathbf{V}(\mathbf{r}) \in \mathbb{C}^{p\times 2}$, $\mathbf{v}(\mathbf{r}; H)$ and $\mathbf{v}(\mathbf{r}; V)$ are used to denote the response to the H and V channels, respectively, or as a formula.

$$\mathbf{V}(\mathbf{r}) = [\mathbf{v}(\mathbf{r}; H), \mathbf{v}(\mathbf{r}; V)]. \tag{8}$$

3. Two-Dimensional Beampattern Synthesis for Polarized Smart Antenna Array

A two-dimensional beamforming method for polarized smart antenna array is proposed in this section. Xiao and Nehorai designed a null and sidelobe polarization for the polarized beampattern [6]. However, the null and polarization controls of the sidelobe are independent, which did not maximize the advantages of polarization isolation and null. SOCP is still adopted to deal with the two-dimensional beamforming for polarized antenna arrays. Different from the previous literature, this section extends it to two-dimensional polarization beamforming. Here, the weight matrix ω is synthesized to generate a beampattern. Suppose a uniform planar array comprises $N \times N$ antennas with an element spacing d (half wavelength), as shown in.

According to the array model shown in Figure 3, the weighting matrix ω is introduced in this section to be the concatenation of all $\omega_{n\times n}$:
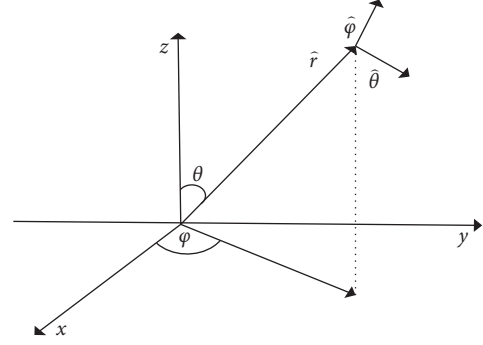

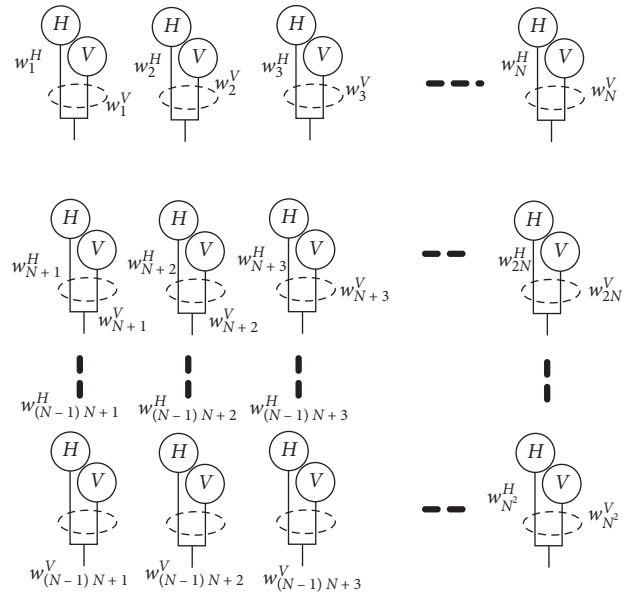FIGURE 2: Spatial coordinate system.

FIGURE 3: Dual-polarized smart antenna array.

$$\boldsymbol{\omega} = \begin{bmatrix} \boldsymbol{\omega}_{11}^T & \boldsymbol{\omega}_{12}^T & \cdots & \boldsymbol{\omega}_{1N}^T \\ \boldsymbol{\omega}_{21}^T & \boldsymbol{\omega}_{22}^T & \cdots & \boldsymbol{\omega}_{2N}^T \\ \vdots & \vdots & \ddots & \vdots \\ \boldsymbol{\omega}_{N1}^T & \boldsymbol{\omega}_{N2}^T & \cdots & \boldsymbol{\omega}_{NN}^T \end{bmatrix}, \tag{9}$$

where

$$\boldsymbol{\omega} = \begin{bmatrix} \boldsymbol{\omega}^H, \boldsymbol{\omega}^V \end{bmatrix}^T. \tag{10}$$

For convenience of calculation, the $N \times N$ matrix ω_{NN}^T is transformed into $1 \times N^2$ column vectors as follows:

$$\boldsymbol{\omega}^H = \begin{bmatrix} \omega_1^H, \omega_2^H, \ldots, \omega_{N^2}^H \end{bmatrix},$$

$$\boldsymbol{\omega}^V = \begin{bmatrix} \omega_1^V, \omega_2^V, \ldots, \omega_{N^2}^V \end{bmatrix}. \tag{11}$$

Given the location of actual element $\mathbf{x}_n$: $1 \le n \le N^2$, which has the N^2 candidate positions, the array response, as a function of spatial direction $\mathbf{r}$, can be expressed as follows:

$$\mathbf{AF}(\mathbf{r}) = \left[e^{-j\psi_1(\mathbf{r})}, e^{-j\psi_2(\mathbf{r})}, \ldots, e^{-j\psi_{N^2}(\mathbf{r})} \right]^T, \tag{12}$$

where $\psi_n(\mathbf{r}) = k\mathbf{r} \cdot \mathbf{x}_n$ and $k = (2\pi/\lambda)$ is the wave number.

Thus, in terms of the vector antenna response $\mathbf{V}(\mathbf{r})$, the $N^2 \times 2$ vector antenna array response is further obtained as follows:

$$\mathbf{A}(\mathbf{r}) = \mathbf{AF}(\mathbf{r}) \otimes \mathbf{V}(\mathbf{r}) = \left[e^{-j\psi_1(\mathbf{r})}\mathbf{V}(\mathbf{r}) \cdots e^{-j\psi_{N^2}(\mathbf{r})}\mathbf{V}(\mathbf{r}) \right]^T. \tag{13}$$

The antenna array response of H and V channels is defined as follows:

$$\begin{aligned} \mathbf{A}(\mathbf{r}; H) &= \mathbf{AF}(\mathbf{r}) \otimes \mathbf{v}(\mathbf{r}; H), \\ \mathbf{A}(\mathbf{r}; V) &= \mathbf{AF}(\mathbf{r}) \otimes \mathbf{v}(\mathbf{r}; V). \end{aligned} \tag{14}$$

The normalized electrical field emitted from the antenna array (ignoring the common carrier and the baseband signal $s(t)$) can be expressed as follows:

$$\mathbf{E}(\mathbf{r}) = \mathbf{A}(\mathbf{r})^T \boldsymbol{\omega}, \tag{15}$$

where $\mathbf{E}(\mathbf{r}; H)$ and $\mathbf{E}(\mathbf{r}; V)$ are used to denote the decomposition of $\mathbf{E}(\mathbf{r})$:

$$\mathbf{E}(\mathbf{r}; H) = \mathbf{A}(\mathbf{r}; H)^T \boldsymbol{\omega}, \tag{16}$$

$$\mathbf{E}(\mathbf{r}; V) = \mathbf{A}(\mathbf{r}; V)^T \boldsymbol{\omega}. \tag{17}$$

Along $\mathbf{r}$, the polarization state can be determined by the ratio between $\mathbf{E}(\mathbf{r}; H)$ and $\mathbf{E}(\mathbf{r}; V)$, and the transmitting power can be expressed as $\|\mathbf{E}(\mathbf{r})\|^2 = |\mathbf{E}(\mathbf{r}; H)|^2 + |\mathbf{E}(\mathbf{r}; V)|^2$:

$$\begin{aligned} \mathbf{E}(\mathbf{r}) &= (\mathbf{AF}(\mathbf{r}) \otimes \mathbf{V}(\mathbf{r}))^T \boldsymbol{\omega} \\ &= \mathbf{V}(\mathbf{r})^T \left[s^H \quad s^V \right]^T, \end{aligned} \tag{18}$$

where ω_n^H and ω_n^V are the complex weights of the horizontal and vertical channels, respectively. $s^H(\mathbf{r})$ and $s^V(\mathbf{r})$ are, respectively, defined as follows:

$$\begin{aligned} s^H(\mathbf{r}) &\triangleq \mathbf{AF}(\mathbf{r})^T \boldsymbol{\omega}^H, \\ s^V(\mathbf{r}) &\triangleq \mathbf{AF}(\mathbf{r})^T \boldsymbol{\omega}^V. \end{aligned} \tag{19}$$

The selection of ω under maximal sidelobe minimization is one of the problems in achieving the following goals.

(1) Maximize the power of the main beam (at direction r_0) and match polarization parameter pair (μ, ν); the region of main beam is denoted by S_m)

(2) Minimize power of sidelobe (this region is denoted by S_r at direction $\mathbf{r}_s$)

(3) A desired null in the directions of interferers (generally located in the sidelobe region and denoted by S_n), which has cross-polarization constraint (α_p, β_p)

Based on above, the polarized beampattern synthesis problem can be formulated as follows:

$$\min_{\mathbf{r}_s \in S_r} \quad \tau$$

$$\text{subject to} \begin{cases} \mathbf{E}(\mathbf{r}_0) = \sqrt{E_0}\, e^{j\phi} \begin{bmatrix} \cos\mu & -\cos\mu \\ \sin\mu & \cos\mu \end{bmatrix} \begin{bmatrix} \cos\nu \\ j\sin\nu \end{bmatrix} \\ \max_{\mathbf{r}_s \in S_r} \left\{ \|\mathbf{E}(\mathbf{r}_s; H)\|^2 + \|\mathbf{E}(\mathbf{r}_s; V)\|^2 \right\} \leq \tau^2; \quad \mathbf{r}_s \in S_r \\ \begin{bmatrix} E^H(\mathbf{r}_n) \\ E^V(\mathbf{r}_n) \end{bmatrix} = \sqrt{P}\, e^{j\phi} \begin{bmatrix} \cos\alpha_p & \sin\alpha_p \\ -\sin\alpha_p & \cos\alpha_p \end{bmatrix} \begin{bmatrix} \cos\beta_p \\ j\sin\beta_p \end{bmatrix} \\ \|\mathbf{E}(\mathbf{r}_n; H)\|^2 + \|\mathbf{E}(\mathbf{r}_n; V)\|^2 \leq \varepsilon^2, \quad \mathbf{r}_n \in S_n. \end{cases} \tag{20}$$

where τ is the optimal solution, which measures the beampattern power gain over the sidelobes and does not depend on the main beam polarization. The third constraint directly determines the polarization of notch and its depth ($\varepsilon = \sqrt{P}$). When ω is a column vector of $1 \times N^2$, the above optimization mode is also applicable to the synthesis of the polarized beampattern for ULA. This condition is a vector optimization problem that is difficult to solve using an optimization algorithm. Thus, this optimization problem is split into two equivalent scalar optimization problems as follows:

Horizontal channel is

$$\min_{\omega^{(H)}} \quad \max_{\mathbf{r}_s \in S_r} |E^H(\mathbf{r}_s)|^2$$

$$\text{subject to} \quad E(\mathbf{r}_m) = (\cos\mu\cos\nu + j\sin\mu\sin\nu)$$

$$E(\mathbf{r}_n) = \boldsymbol{\varepsilon}(p - c, q - c) \cdot (\cos\alpha_p\cos\beta_p + j\sin\alpha_p\sin\beta_p), \quad \mathbf{r}_n \in S_n. \tag{21}$$

Vertical channel is

$$\min_{\boldsymbol{\omega}^{(V)}} \quad \max_{\mathbf{r}_s \in S_r} |E^V(\mathbf{r}_s)|^2$$

$$\text{subject to} \quad E(\mathbf{r}_0) = (-\sin\mu\cos\nu + j\cos\mu\sin\nu)$$

$$E(\mathbf{r}_n) = \boldsymbol{\varepsilon}(p - c, q - c) \cdot (-\sin\alpha_p\cos\beta_p + j\cos\alpha_p\sin\beta_p), \quad \mathbf{r}_n \in S_n. \tag{22}$$

In (21) and (22), ε is called the null concave matrix for polarized smart antenna array and is introduced as follows:

$$\boldsymbol{\varepsilon} = \begin{bmatrix} 20\lg \varepsilon_{(p-c,q-c)} & 20\lg \varepsilon_{(p-c+1,q-c)} & \cdots & 20\lg \varepsilon_{(p+c,q-c)} \\ 20\lg \varepsilon_{(p-c,q-c+1)} & 20\lg \varepsilon_{(p-c+1,q-c+1)} & \cdots & 20\lg \varepsilon_{(p+c,q-c+1)} \\ \vdots & \vdots & \ddots & \vdots \\ 20\lg \varepsilon_{(p-c,q+c)} & 20\lg \varepsilon_{(p-c+1,q+c)} & \cdots & 20\lg \varepsilon_{(p+c,q+c)} \end{bmatrix},$$

(23)

where $\mathbf{p} = (p - c, \ldots, p - 1, p, p + 1, \ldots, p + c)$, $\mathbf{q} = (q - c, \ldots, q - 1, q, q + 1, \ldots, q + c)$, and c is a constant. The above optimized problem is convex and is also an SOCP problem.

4. Sparse Array Design for Polarized Smart Antenna

Pattern performance and polarization constraint for the polarized smart antenna must be considered in the sparse process of antenna array [21]. The optimization model must be a multiconstraint problem, including the unequal constraints, to accomplish both purposes. Following [22, 23], a two-stage design approach is adopted to deal with the sparse array design for polarized smart antenna. In the first stage, the weight matrix ω is synthesized to generate a pattern for $N \times N$ polarized antenna array with an N^2 antenna element, as mentioned in Section 3. In the second stage, the element positions of the full array are treated as candidate positions that are selected by a sparse array with M antenna elements.

Mean square error of polarization matching in interest area (PMSE) is defined as an objective function, whereas the peak sidelobe levels (PSLLs) minimization of sparse array design is another objective function [24]. This optimization problem of PMSE can be constructed as follows:

$$f(x) = \frac{1}{K} \sum_{k=1}^{K} \left\{ \left[\boldsymbol{\alpha}(\theta_k, \varphi_k) - \boldsymbol{\alpha}_{\text{best}}(\theta_k, \varphi_k) \right]^2 + \left[\boldsymbol{\beta}(\theta_k, \varphi_k) - \boldsymbol{\beta}_{\text{best}}(\theta_k, \varphi_k) \right]^2 \right\},$$

(24)

where K is the number of sampling points in the far-field area for the optimal polarized beampattern.

The optimization problem for a sparse antenna array design aimed at polarization matching to control the designed polarization as desired in the interesting region can be written as follows:

$$\min \quad f(\mathbf{x})$$

$$\text{subject to} \begin{cases} -N_x \le m \le N_x, \quad -N_y \le n \le N_y \\[2mm] a(N_x, 0) = 1, a(-N_x, 0) = 1 \\[2mm] a(0, -N_y) = 1, a(0, N_y) = 1 \\[2mm] \text{PSLLs} - \delta < 0 \\[2mm] \sum_{m=-N_x}^{N_x} \sum_{n=-N_y}^{N_y} a_{mn} = T \\[2mm] \left| \dfrac{E(\theta_{i-c}, \varphi_{j-c})}{\text{FF}_{\max}} \right| \le \varepsilon(i - c, j - c), \quad i, j = 1, 2, \ldots. \end{cases}$$

(25)

where the first three constraints fix the four sides of the antenna aperture, δ is the tolerance value for PSLLs in the fourth constraint (which is an inequality constraint), the fifth constraint sets the actual number of elements (T), and

the last constraint realizes the depth and polarization of null ($\text{FF}_{\max}$ is the peak of the main lobe). Following the idea of multiobjective optimization, the inequality constraint can be regarded as another objective function in the evolution process [24]. This constraint can be optimized in parallel implementation as follows:

$$\min \quad (f_1(\mathbf{x}), f_2(\mathbf{x}))$$

$$\text{subject to} \begin{cases} -N_x \le m \le N_x, \quad -N_y \le n \le N_y \\[2mm] a(N_x, 0) = 1, a(-N_x, 0) = 1 \\[2mm] a(0, -N_y) = 1, a(0, N_y) = 1 \\[2mm] \sum_{m=-N_x}^{N_x} \sum_{n=-N_y}^{N_y} a_{mn} = T \\[2mm] \left| \dfrac{E(\theta_{i-c}, \varphi_{j-c})}{\text{FF}_{\max}} \right| \le \varepsilon(i - c, j - c), \quad i, j = 1, 2, \ldots. \end{cases}$$

(26)

where $f_1(\mathbf{x})$ is defined in (23) and $f_2(\mathbf{x}) = \text{PSLLs}$. Inspired by [23], the MODE algorithm is suitable for this kind of multiobjective optimization problem and is designed to handle a multiset of solutions in a single iteration. In the multiobjective domain, the MODE aims to identify a set of Pareto optimal solutions to operate the selection of the best individual for the mutation (Appendix A). At the end of the

evolutionary search, the nondominated solution archive is passed through a dominance filter to yield the global near-Pareto-optimal frontier (Appendixes B and C) [23, 25]. The individual representation (Initial and Coding) needs to be explained as follows.

4.1. Initial. Let $x_{i,G}^j$ denote the initial value of the j parameter in the ith population at generation G, which is shown as follows:

$$x_{i,G}^j = \text{rand}(0,1) \cdot \left(x_{\max}^j - x_{\min}^j \right) + x_{\min}^j, \quad i = 1, \ldots, \text{NP}, j = 1, \ldots, D, \tag{27}$$

where $D = N^2 - 4$, and $\text{rand}(0,1)$ is a uniformly distributed random variable within the range $[0,1]$, and $x_{\max}^j$ and $x_{\min}^j$ are the lower and upper bounds of the jth variable parameter, respectively. The individual in the ith population at generation G can be obtained in its vector form as follows:

$$\mathbf{x}_{i,G} = \left[x^1, x^2, \ldots, x^D \right]. \tag{28}$$

4.2. Coding. The initial value of the antenna position is set as the partition points of a planar array aperture. The random perturbation is controlled by $x_{i,G}$, and binary coded $\mathbf{p}_s$ denotes the location of actual elements, which is shown as follows:

$$\mathbf{p}_s(n,n) = \text{sort}(\mathbf{x})^{\text{T}}, \quad n = 1, \ldots, N^2 - 4, \tag{29}$$

where $\text{sort}(\cdot)$ denotes the real variables that are sorted by size as integer variables converted into binary codes.

The whole process of sparse array design using MODE algorithm can be summarized as follows (Algorithm 1).

Steps 3–5 evaluate the fitness function at these 2NP solutions at each generation G, select the NP fittest solutions via fast nondominated sorting, and store them in the current population pop_c. In our approach, fast nondominated sorting is applied to guarantee that the population maintains its original size, and the nondominated solutions in the population are identified at each generation of the evolution process. The nondominated solutions are saved in the advanced population that corresponds to the feasible solution [26]. Otherwise, the infeasible solution is reserved in current population.

5. Numerical Example

The simulation results are presented in this section to illustrate the effectiveness of the proposed method. Considering the preliminary results reported in [6, 9], the application of the SOCP to polarized beampattern synthesis must be investigated. Thus, the polarized beampattern synthesis is introduced for polarized smart antenna based on ULA in Example 1. This example highlights the continuity and innovation of the proposed method. The cross-polarization is added on the null of the beampattern to improve the capability of interference suppression in the sidelobe region, which is different from [6]. Example 2 synthesizes the 2D polarization beampattern and obtains the corresponding

polarization state for the polarized smart antenna array. Example 3 realizes the sparse array design of the 2D polarized smart antenna array.

5.1. Polarized Beampattern with a Null that Has Cross-Polarization Based on ULA. Assume that a strong interference is located at an azimuth angle of $\theta = 23°$, and its polarization state can be depicted with polarization ellipse parameters of $\alpha = 80°$ and $\beta = 25°$. Thus, a desired null (SLL ≤ -50 dB) with ($\alpha = -10°$ and $\beta = 25°$) that is located at $\theta \in (20°, 25°)$ must be designed. The entire angle area is $\theta \in (-90°, 90°)$ with $1°$ angular spacing (such that $K = 181$). Assume a strong interference is at the azimuth angle of $\theta = 23°$. The polarization state of this strong interference can be depicted with polarization ellipse parameters of $\alpha = 80°$ and $\beta = 25°$. The desired null (SLL $= -50$ dB) with $\alpha = -10°$ and $\beta = 25°$, which is located at $\theta = [20°, 25°]$, must be designed.

Figure 4(a) depicts a polarized beampattern with one desired polarization. The result shows that the polarization can be controlled such that the interference of the known source is isolated, and the gain of the main lobe is 16 dB. Figure 4(b) presents that the desired polarization ellipse parameter is a constant in the entire angle region. Figure 5(a) depicts a polarized beampattern with the desired null. The result also shows that the depth of the obtained null can reach -24 dB compared with the maximum peak sidelobe level. However, Figure 5(b) displays that the curve of the polarization ellipse parameter in the entire angle area is not constant, except for the main lobe region; that is, no law exists.

Figure 6(a) shows the beampattern of the proposed method. Figure 6(b) displays that the curve of the polarization ellipse parameter in the entire angle area is not constant; that is, no law exists. However, this curve meets the interests in that region, such as the main lobe and jamming direction. Thus, all these findings justify the efforts to prevent jamming due to polarization mismatch.

5.2. Two-Dimensional Beampattern Synthesis for Polarized Smart Antenna Array. Similar to Example 1, SOCP is applied to optimize the 2D polarized beamform as mentioned in Section 3. The only difference from the previous example is that the variable is no longer a column vector but a matrix. Thus, the weight matrix must be transformed into column vectors again. Assume that a planar array of 10×10 ($N = 10$) is synthesized and satisfies the following constraints: (1) The distance between any pair of elements is equal to $d_c = 0.5\lambda$. (2) All elements are allocated on a fixed aperture of $4.5\lambda \times 4.5\lambda$. (3) The main beam is targeted at $\varphi = 20°$ and $\theta = 20°$ with beam width of $7.5°$ and polarization constraint $(\mu, \nu) = (10°, 20°)$. (4) The null is located at $\varphi \in (60°, 63°)$ and $\theta \in (60°, 62°)$ with the polarization constraint $(\alpha_i, \beta_i) = (25°, 35°)$. Therefore, the coordinate vector of the null concave in the sidelobe region is equal to $\mathbf{p} = (60°, 61°, 62°)$, $\mathbf{q} = (60°, 61°, 62°)$, and the depth is $20 \cdot \lg\varepsilon = 60$ dB($\varepsilon = 0.001$). According to the optimization model defined by equations (16) and (17), CVX MOSEKY

Input: ω, NP, M, N, $G\_$ max
Step 1: **initial**. $a(N_x, 0) = 1, a(-N_x, 0) = 1, a(0, -N_y) = 1, a(0, N_y) = 1;$ $G = 1, \ldots, G\_\text{max} x_{i,G}^j = \text{rand}(0,1)$, $i = 1, \ldots, NP$, $j = 1, \ldots, N^2$
Step 2: **coding**. $\mathbf{x}_{i,G} \longrightarrow \mathbf{p}_s$, $f_1(x)$ is defined in (24), $f_2(x) = \text{PSLLs}(\mathbf{x})$
For $p \longleftarrow 1$ to NP do
  Step 3: **mutation**. Randomly select three distinct individuals, $\mathbf{x}_{r1}$, $\mathbf{x}_{r2}$, and $\mathbf{x}_{r3}$, who are all different from the target individual.
Generate a perturbed individual $\mathbf{U}_i$ by $\mathbf{U}_{i,G+1} = \mathbf{x}_{tb,G} + F(\mathbf{x}_{r2,G} + \mathbf{x}_{r3,G})$
  The scaling factor $F \in [0, 2]$ is constant. $\mathbf{x}_{tb,G}$ denotes the best individuals among the three individuals, which is mean that the one has best fitness function value
  Step 4: **crossover**. The objective function value of each trial vector $f(\mathbf{v}_{i,G})$ is compared with that of its corresponding target vector $f(\mathbf{x}_{i,G})$. The vector with the smaller fitness value will be retained in the next generation. Generate a trial individual as follows:
$$\mathbf{v}_{i,G+1} = \begin{cases} \mathbf{v}_{i,G}, & if \quad f(\mathbf{v}_{i,G}) < f(\mathbf{x}_{i,G}), \\ \mathbf{x}_{i,G}, & \text{otherwise.} \end{cases}$$
  calculate the fitness value of $\mathbf{V}_{i,G+1}$, $p = p + NP$
  Step 5: **Pareto dominance**
  If ($\mathbf{V}_i$ dominates $\mathbf{x}_i$)
    replace $\mathbf{x}_i$ by $\mathbf{V}_i$ in the current population pop_c, and then add $\mathbf{x}_i$ to the advanced population pop_a
  Else
    add $\mathbf{V}_i$ to the advanced population pop_a
  End
end
  NP fittest solutions is select in every fast nondominated sorting and save them in pop_c; $\mathbf{p}_{s,\text{best}}$ is the $\mathbf{p}_s$ with the lowest fitness value of $f_1(x)$
Output: $\mathbf{p}_{s,\text{best}} \longrightarrow \mathbf{A}_s \longrightarrow \mathbf{p} = \mathbf{A}_s^H \omega$

ALGORITHM 1: MODE algorithm.

--- H-channel
······ V-channel
—— Vector

(a)

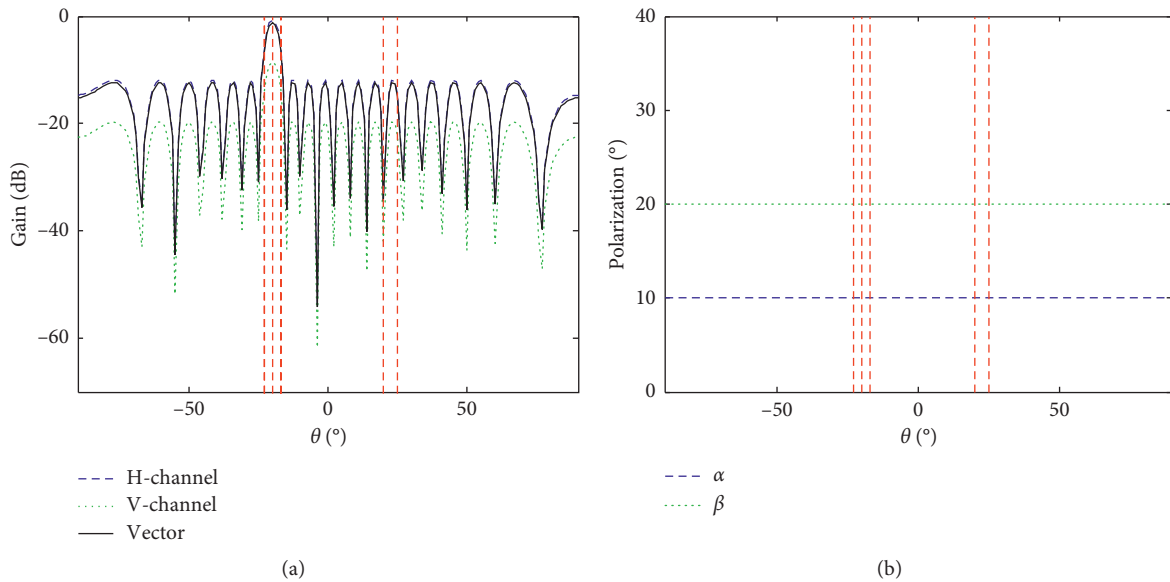--- α
······ β

(b)

FIGURE 4: First method of polarized beampattern in [6]. (a) Beampattern. (b) Polarization.

solver is used to solve the two equivalent scalar problems [27]. The following results are obtained.

For clarity, 3D and contour figures represent the optimized beampattern. A null concave with the average depth of -91.5 dB is located at $\theta \in (60°, 62°)$ and $\phi \in (60°, 62°)$ in Figure 7. Compared to the maximum peak sidelobe (-16.5 dB), the polarized beampattern obtained a suppression gain with -75 dB. α and β are also represented by a surface to verify the polarization state of 2D polarized beampattern, as shown in Figure 8. Different from the previous example, the polarization state of interesting area cannot be directly observed from the curved surface. However, if the tangent of the surface is used for representation, then the polarization state values of null concave cannot be fully expressed. Thus, a table is used to express the corresponding polarization state values at several sampling points of interesting areas, as shown in Tables 1 and 2.

Tables 1 and 2 suggest that the polarization parameter pair (α, β) is consistent with the experimental setting, where

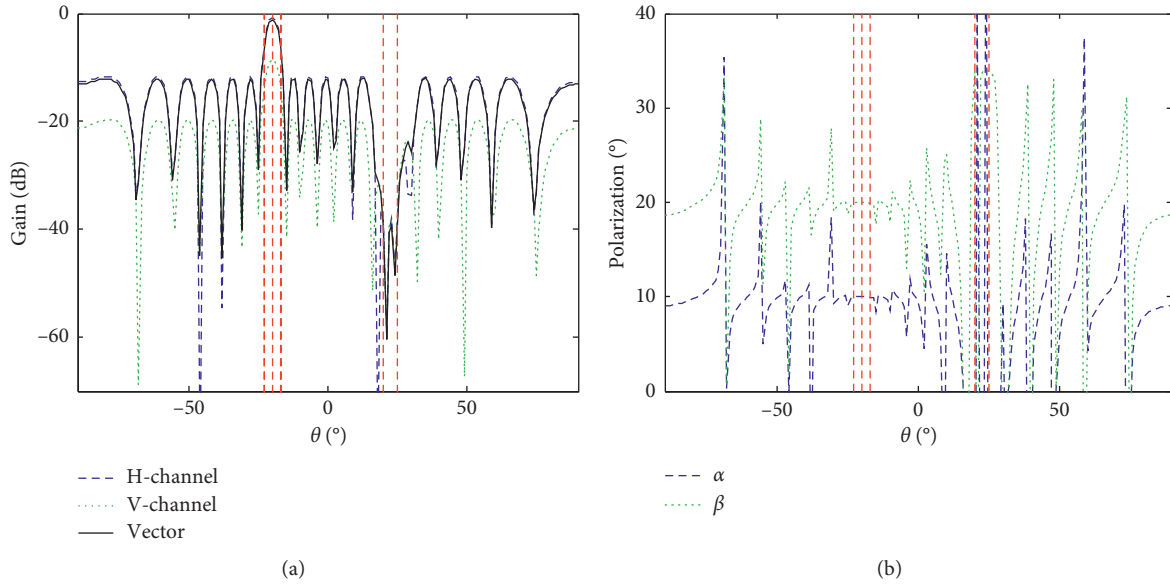(a)   (b)

FIGURE 5: Second method of polarized beampattern in [6]. (a) Beampattern. (b) Polarization.

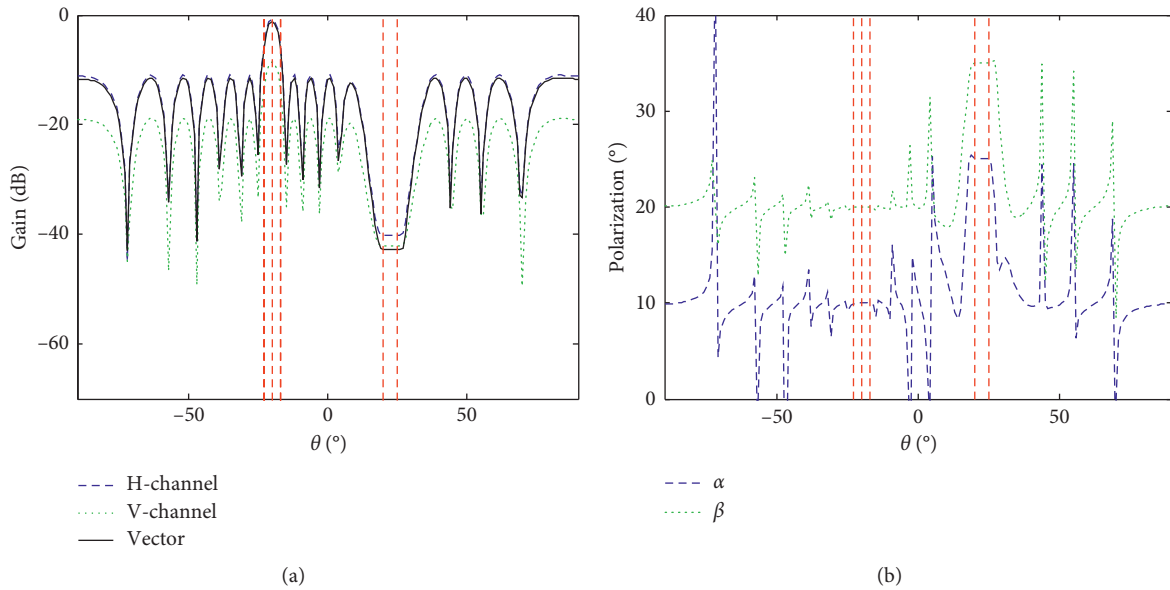(a)   (b)

FIGURE 6: Proposed method of polarized beampattern. (a) Beampattern. (b) Polarization.

p and q, respectively, refer to the sampling points of the main lobe and null concave, as defined in (18). Similar to Example 1, the constraint of polarization matching cannot guarantee the polarization state outside the region of interest.

5.3. Sparse Array Optimization of Polarized Smart Antenna Using MODE. The MODE algorithm is applied for sparse antenna array design to verify the effectiveness of the method mentioned in Section 4. Given its particularity, this optimization problem is suitable for the multiobjective differential evolution algorithm. Thus, we only apply the multiobjective differential evolution algorithm to its sparse

array optimization. Herein, the sparse rate is set as 75%. Thus, $M = 75$ antenna elements selected from 100 candidate positions ($N = 10 \times 10$ planar array) are used. Other simulation conditions remain the same as those in Example 2. The parameters of MODE are defined and applied as follows:

(1) Population size: NP = 100

(2) Initial range: $x_{max} = 1, x_{min} = 0$

(3) Mutation probability: $F = 0.8$

(4) Crossover probability: CR = 0.3

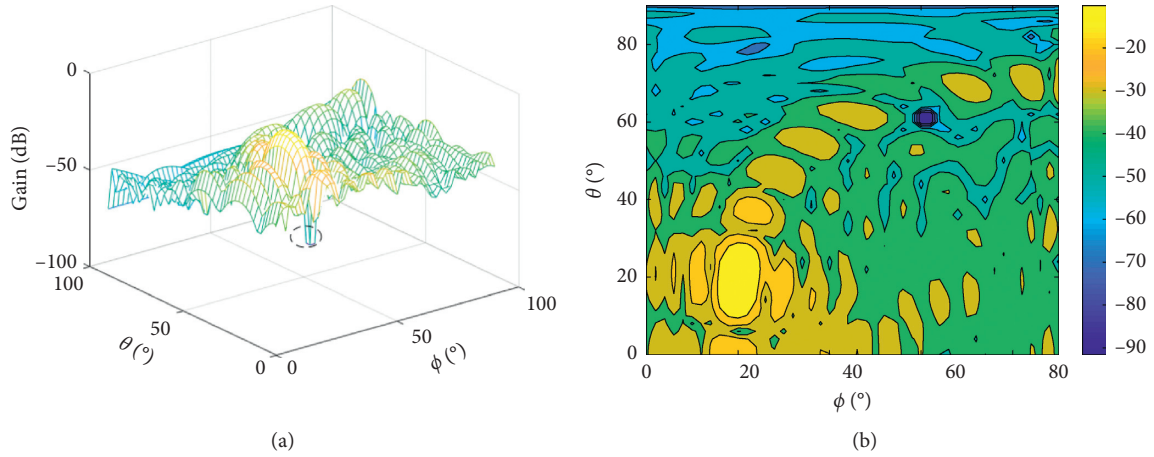(5) Maximum number of iterations: $G\_max = 200$

FIGURE 7: Polarized beampattern using the proposed method. (a) The 3D polarized beampattern. (b) The contour of polarized beampattern.
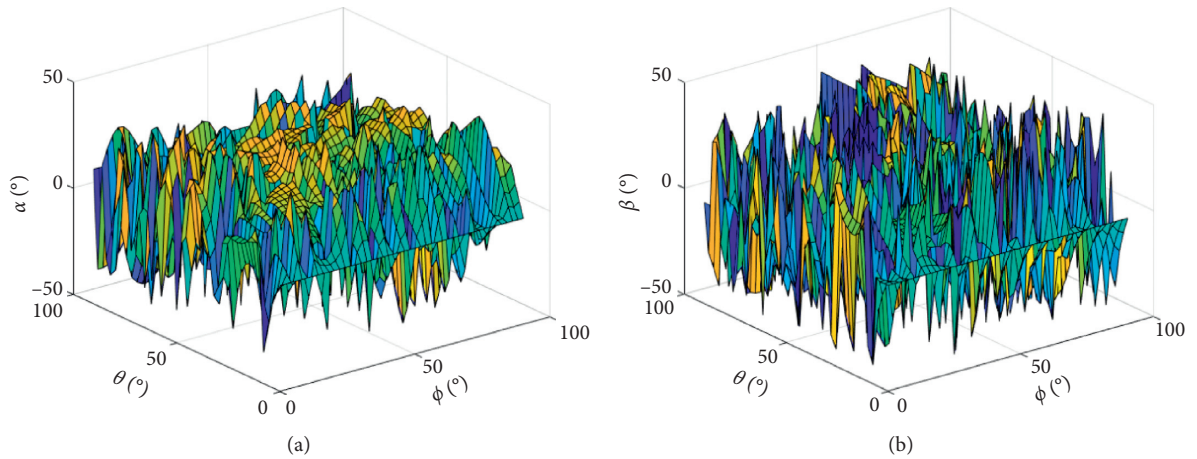

FIGURE 8: The surface of polarization parameter pair using the proposed method. (a) Orientation angle. (b) Ellipse angle.

TABLE 1: Polarization state in the main lobe.

Sampling points	1	2	3	4	5	6	7	8	9
p	19	19	19	20	20	20	21	21	21
q	19	20	21	19	20	21	19	20	21
μ	9.80	9.90	8.05	10.00	10.00	9.01	8.05	9.20	9.80
ν	19.79	19.90	19.99	20.97	20.97	20.00	20.05	21.95	21.70

TABLE 2: Polarization state in the null.

Sampling points	1	2	3	4	5	6	7	8	9
p	60	60	60	61	61	61	62	62	62
q	60	61	62	60	61	62	60	61	62
α_i	24.79	24.90	24.99	25.00	25.00	25.00	25.05	24.95	24.70
β_i	34.89	33.34	36.89	35.00	35.00	37.90	34.56	36.90	39.00

SOCP is repeated to establish the optimum covariance matrix ω, and the evolution process continues until the maximum number of iterations for testing convergence is reached. The results are shown as follows.

The red asterisks in Figure 9(a) record all the infeasible solution sets, and the black diamonds represent the feasible solution sets in one run. To balance the performance of both PMSE and PSLL, the solution (PMSE = 0.0086 and
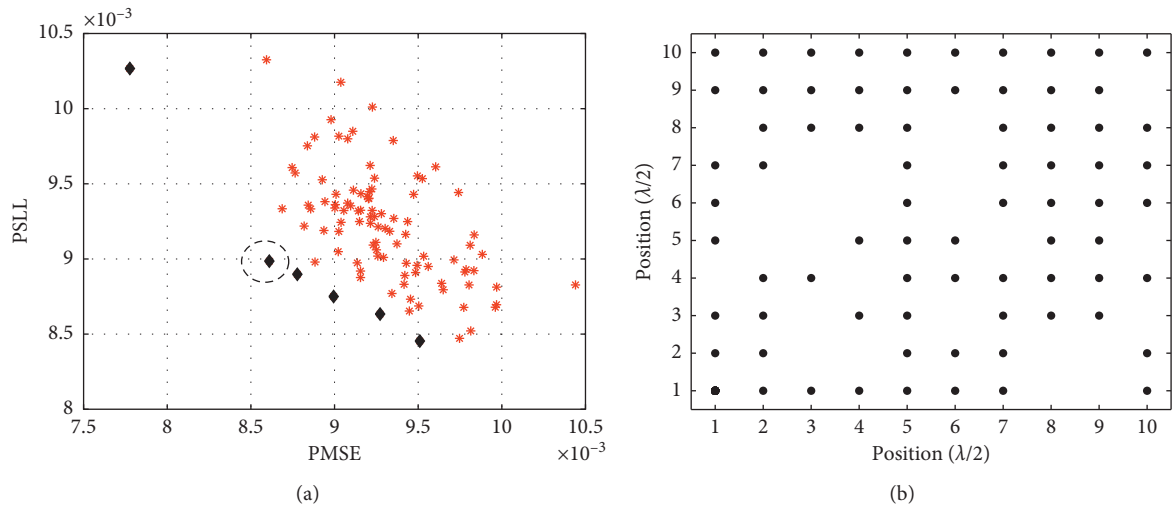
(a)

(b)

FIGURE 9: Pareto fronts produced by MODE. (a) Pareto fronts. (b) Position of antenna.
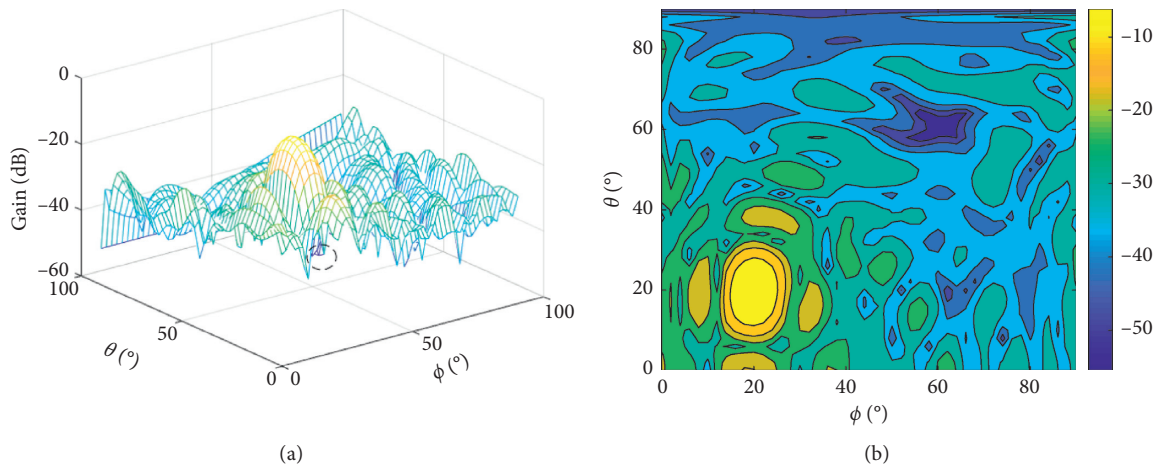

(a)

(b)

FIGURE 10: Beampattern produced by MODE. (a) The 3D polarized beampattern. (b) The contour of polarized beampattern.
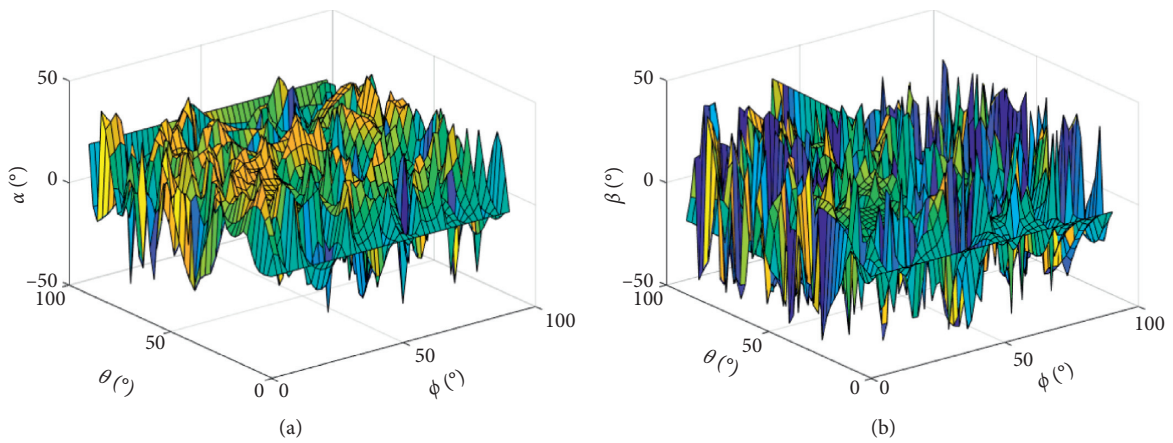

(a)

(b)

FIGURE 11: The surface of polarization parameter pair using the MODE. (a) Orientation angle. (b) Ellipse angle.

TABLE 3: Polarization state in the region of the main lobe.

Sampling points	1	2	3	4	5	6	7	8	9
p	19	19	19	20	20	20	21	21	21
q	19	20	21	19	20	21	19	20	21
μ	9.32	8.85	9.2621	10.91	10.00	10.07	10.00	10.01	10.80
ν	19.85	20.00	20.05	19.86	20.00	20.00	21.11	20.00	21.30

TABLE 4: Polarization state in the region of null concave.

Sampling points	1	2	3	4	5	6	7	8	9
p	60	60	60	61	61	61	62	62	62
q	60	61	62	60	61	62	60	61	62
α_i	23.79	25.49	24.50	23.30	24.20	26.11	25.52	28.7782	25.2064
β_i	32.15	31.89	32.25	35.04	35.46	34.24	34.20	35.00	36.56

TABLE 5: Performance of MODE in 10 runs.

Algorithm: MODE	Index of runs									
	1st	2nd	3rd	4th	5th	6th	7th	8th	9th	10th
PMSE	0.0086	0.0086	0.0087	0.0086	0.0086	0.0086	0.0086	0.0086	0.0086	0.0086
PSLLs	0.0090	0.0090	0.0091	0.0090	0.0090	0.0091	0.0091	0.0090	0.0090	0.0089
Iterations	27	27	27	27	27	27	28	25	28	26
Runtime	15/00	15/04	15/66	15/20	15/25	15/23	15/12	15/00	15/27	15/25

PSLL = 0.009) marked by the dotted circle should be the best choice in experience. Figure 9(b) shows the selected antenna positions corresponding to the best solution, and the sparse rate is set to 75%. In Figure 10, it is easy to see that the average PSLL is about −10 dB, and the depth of null obtained is −50 dB. Those performances are worse than those in Figure 7. This finding is due to the decrease in the number of array elements, which leads to increased sidelobe levels. However, the performance of polarization matching in the interesting area and the PSLLs outside the beampattern is balanced. The restriction for the polarization matching in this study is to maintain the best approximation of polarization matching while keeping the sidelobe level as flat as possible, as shown in Figures 9 and 10. Figure 11 shows the surface value of the polarization ellipse parameter that uses the MODE. As previously described, we still cannot see the polarization state of interest region in Figure 11. Thus, the corresponding polarization states are shown in Tables 3 and 4, respectively.

Table 5 shows the chosen PMSE and PSLLs in ten independent runs.

Table 5 summarizes the results of MODE in 10 runs. The highest PMSE is below 0.0091, whereas all PSLLs slightly fluctuate around 0.009. This finding suggests the stability of PSLLs obtained using MODE. MODE has almost the same running time as DE despite the constraint added by the former to the optimization problem. Moreover, MODE has a simpler algorithm structure than that of DE. These arguments justify efforts to prevent PMSE.

6. Conclusions

A novel two-stage design approach for the sparse antenna array design of 2D polarized smart antenna arrays is proposed in this work. A new model of optimal polarized beampattern optimization problem based on SOCP is formulated in the first stage. A multiobjective optimization problem for sparse arrays, which can be solved by MODE, is then proposed in the second stage. Compared with the existing method in [6], the cross-polarization on the null is constrained to maximize the capability of interferer suppression while retaining the polarization matched reception in the main lobe. This method is extended to the two-dimensional polarized antenna array. Given the substantial hardware cost, the MODE algorithm based on Pareto technique is proposed to obtain the sparse array. In this algorithm, the PMSE in the interest area is presented as another objective function to be optimized. The simulation results reveal that MODE outperforms other algorithms in terms of sparse arrays while maintaining polarization matching performance.

Although only beampattern synthesis and sparse array for polarized smart antenna array are considered, the effect of the matching reception and interference suppression is not evaluated in practical application. The extension of this method to the detection and interference suppression of systems is part of future studies.

Appendix

A. Opposition-Based Learning

Proof. The opposition-based learning is introduced to generate opposite solutions in the initialization to increase the chances of starting with the fittest solution [20], which can be expressed as follows:

$$y_i^j = \left(x_{\max}^j + x_{\min}^j\right) - x_i^j, \quad i = 1, \ldots, \text{NP}, j = 1, \ldots, D.$$
(A.1)

□

B. Pareto Dominance

Proof. A solution x_1 is said to dominate another solution x_2 under the following conditions:

(1) $\forall m \in (1, \ldots, M_{\text{obj}}): f_m(x_1) \leq f_m(x_2)$

(2) $\exists m \in (1, \ldots, M_{\text{obj}}): f_m(x_1) < f_m(x_2)$

where M_{obj} is the number of objective functions and $f_m(\cdot)$ is the corresponding fitness function. Any individual that is not dominated by any other member is considered nondominated.   □

C. Fast Nondominated Sorting

Proof. Assume a Pareto optimal set denoted by S. n_p denotes the number of dominated solutions, while S_p is a set of solutions dominated by the solution p [20].

For every solution p in S, both n_p and S_p are calculated. All solutions in the first nondominated front F_1 clear their domination count to zero. Afterwards, when $n_p = 0$, each solution p visits each member q of its set S_p, and $n_p = n_p - 1$. Any member q is saved in a separate list P. These members belong to the second nondominated front F_2. Each member of P and the third front F_3 are identified. This process continues until all fronts have been identified.   □

Data Availability

The data used to support the findings of this study are available from the corresponding author upon request.

Conflicts of Interest

The authors declare no conflicts of interest regarding the publication of this article.

Acknowledgments

References

[1] C. B. Dietrich, W. L. Stutzman, B.-Ki Kim et al., "Smart antennas in wireless communications: base-station diversity and handset beamforming," *Antennas and Propagation Magazine IEEE*, vol. 42, no. 5, pp. 42–151, 2000.

[2] A. Alexiou and M. Haardt, "Smart antenna technologies for future wireless systems: trends and challenges," *IEEE Communications Magazine*, vol. 42, no. 9, pp. 90–97, 2004.

[3] F. R. . Castella, "Adaptive antenna nulling for a phased array monopulse radar," in *Proceedings of the International Conference of the 1992 IET Radar*, Cambridge , UK, October 1992.

[4] V. Tocca, D. Vigilante, L. Timmoneri et al., "Adaptive beamforming algorithms performance evaluation for active array radars," in *Proceedings of the IEEE Radar Conference (RadarConf18)*, Oklahoma City, OK, USA, April 2018.

[5] N. H. Noordin, W. Zhou, A. O. El-Rayis et al., "Single-feed polarization reconfigurable patch antenna," *Progress in Electromagnetics Research B*, vol. 54, no. 54, pp. 1-2, 2012.

[6] J. J. Xiao and A. Nehorai, "Optimal beampattern synthesis of a polarized array. statistical signal processing, SSP '07," in *Proceedings of the IEEE/SP 14th Workshop on IEEE*, St. Louis, MO, USA, May 2007.

[7] P. Jacob, A. S. Madhukumar, and A. Alphones, "Interference mitigation through cross polarized transmission in femto-macro network," *IEEE Communications Letters*, vol. 17, no. 10, pp. 1940–1943, 2013.

[8] A. Ali, H. Liang, and S. Shetty, "Polarized beamforming for enhanced countermeasure of wireless jamming attacks," in *Proceedings of the IEEE 35th International Performance Computing and Communications Conference (IPCCC)*, IEEE, Las Vegas, NV, USA, December 2016.

[9] J.-J. Jin-Jun Xiao and A. Nehorai, "Optimal polarized beampattern synthesis using a vector antenna array," *IEEE Transactions on Signal Processing*, vol. 57, no. 2, pp. 576–587, 2009.

[10] S. M. Bowers, A. Safaripour, and A. Hajimiri, "Dynamic polarization control," *IEEE Journal of Solid-State Circuits*, vol. 50, no. 5, pp. 1224–1236, 2015.

[11] Y. Lu, Y. Xu, Y. Huang, and Z. Liu, "Diversely polarised antenna-array-based narrowband/wideband beamforming via polarisational reconstruction matrix inversion," *IET Signal Processing*, vol. 12, no. 3, pp. 358–367, 2018.

[12] P. Xie, g.-m. Wang, H. Li et al., "A dual-polarized two-dimensional beam steering fabry-pérot cavity antenna with a reconfigurable partially reflecting surface," *IEEE Antennas & Wireless Propagation Letters*, vol. 16, no. 1, p. 1, 2017.

[13] M. V. Komandla, "Investigations on dual slant polarized cavity-backed massive MIMO antenna panel with beamforming," *IEEE Transactions on Antennas and Propagation*, vol. 65, no. 12, pp. 6794–6799, 2017.

[14] K. Chen, X. Yun, Z. He, and C. Han, "Synthesis of sparse planar arrays using modified real genetic algorithm," *IEEE Transactions on Antennas and Propagation*, vol. 55, no. 4, pp. 1067–1073, 2007.

[15] C. Chuan Lin, A. Anyong Qing, and Q. Quanyuan Feng, "Synthesis of unequally spaced antenna arrays by using differential evolution," *IEEE Transactions on Antennas and Propagation*, vol. 58, no. 8, pp. 2553–2561, 2010.

[16] D. G. Kurup, M. Himdi, A. Rydberg et al., "Synthesis of uniform amplitude unequally spaced antenna arrays using the differential evolution algorithm," *IEEE Transactions on Antennas and Propagation*, vol. 51, no. 9, pp. 2210–2217, 2003.

[17] R. Bhattacharya, T. K. Bhattacharyya, and R. Garg, "Position mutated hierarchical particle swarm optimization and its application in synthesis of unequally spaced antenna arrays," *IEEE Transactions on Antennas and Propagation*, vol. 60, no. 7, pp. 3174–3181, 2012.

[18] D. Caratelli and M. C. Vigano, "A novel deterministic synthesis technique for constrained sparse array design problems," *IEEE Transactions on Antennas and Propagation*, vol. 59, no. 11, pp. 4085–4093, 2011.

[19] R. Farmani and J. A. Wright, "Self-adaptive fitness formulation for constrained optimization," *IEEE Transactions on Evolutionary Computation*, vol. 7, no. 5, pp. 445–455, 2003.

[20] A. Anders, J. Andersson, and J.-O. Aidanpaa, "Constrained optimization based on a multiobjective evolutionary," in *Proceedings of the 2003 Congress on Evolutionary Computation*, Canberra, ACT, Australia, December 2003.

[21] A. B. Smolders, S. J. Geluk, and A. C. F. Reniers, "Circularly polarized sparse arrays realized by randomly rotated linearly polarized antennas," *IEEE Antennas & Wireless Propagation Letters*, vol. 99, p. 1, 2017.

[22] Z. Cai and Y. Wang, "A multiobjective optimization-based evolutionary algorithm for constrained optimization," *IEEE Transactions on Evolutionary Computation*, vol. 10, no. 6, pp. 398–417, 2006.

[23] Z.-k. Chen, Y. Feng-Gang, Q. Xiao-Lin, and Z. Yi-Nan, "Sparse antenna array design for MIMO radar using multi-objective differential evolution," *International Journal of Antennas and Propagation*, vol. 2016, Article ID 1747843, 12 pages, 2016.

[24] F. Xue, A. C. Sanderson, and R. J. Graves, "Pareto-based Multi-objective differential evolution," in *Proceedings Of The 2003 Congress On Evolutionary Computation*, Canberra, Australia, December 2003.

[25] M. Ali, P. Siarry, and M. Pant, "An efficient differential evolution based algorithm for solving multi-objective optimization problems," *European Journal of Operational Research*, vol. 217, pp. 404–416, 2012.

[26] S. K. Goudos and J. N. Sahalos, "Pareto optimal microwave filter design using multiobjective differential evolution," *IEEE Transactions on Antennas and Propagation*, vol. 58, no. 1, pp. 132–144, 2010.

[27] CVX Research Inc: sedumi_1.3 toolbox, 2014, http://cvxr.com.